SUBMITTED TO APJ, FEBRUARY, 2016
Preprint typeset using LaTeX style emulateapj v. 12/16/11

arXiv:1602.01099v1 [astro-ph.GA] 2 Feb 2016

HIERARCHICAL GALAXY GROWTH AND SCATTER IN THE STELLAR MASS - HALO MASS RELATION

MENG GU[1], CHARLIE CONROY[1] AND PETER BEHROOZI[2, 3, 4]

Submitted to ApJ, February, 2016

ABSTRACT

The relation between galaxies and dark matter halos reflects the combined effects of many distinct physical processes. Observations indicate that the $z = 0$ stellar mass-halo mass (SMHM) relation has remarkably small scatter in stellar mass at fixed halo mass ($\lesssim 0.2$ dex) with little dependence on halo mass. We investigate the origins of this scatter by combining N-body simulations with observational constraints on the SMHM relation. We find that at the group and cluster scale ($M_{\rm vir} > 10^{14} M_\odot$) the scatter due purely to hierarchical assembly is ≈ 0.16 dex, which is comparable to recent direct observational estimates. At lower masses, mass buildup since $z \approx 2$ is driven largely by in-situ growth. We include a model for the in-situ buildup of stellar mass and find that an intrinsic scatter in this growth channel of 0.2 dex produces a relation between scatter and halo mass that is consistent with observations from $10^{12} M_\odot < M_{\rm vir} < 10^{14.75} M_\odot$. The approximately constant scatter across a wide range of halo masses at $z = 0$ thus appears to be a coincidence as it is determined largely by in-situ growth at low masses and by hierarchical assembly at high masses. These results indicate that the scatter in the SMHM relation can provide unique insight into the regularity of the galaxy formation process.

Keywords: galaxies: evolution, galaxies: halos

1. INTRODUCTION

Under the widely accepted cold dark matter model, the assembly history of galaxies is largely driven by the hierarchical growth of the underlying dark matter structures (e.g., White & Rees 1978; Peebles 1982; Blumenthal et al. 1984; White & Frenk 1991). In the past several decades, increasingly accurate cosmological simulations of dark matter halos have enabled detailed study of the structure formation process and has improved our understanding of the statistics of dark matter halos and their evolution (e.g., Springel 2005; Klypin et al. 2011).

However, the galaxy formation process is much more complicated than the cosmological growth of dark matter halos due to a multitute of baryonic processes. In addition to the hierarchical assembly history of dark matter structures, star formation, feedback from stars and supermassive accreting black holes shape the galaxies we see today. Many of these processes are not yet fully understood. Observed scaling relations of galaxies are important to disentangle this complex situation and constrain galaxy formation models. Scaling relations like the star-formation "main sequence" (González et al. 2010; Noeske et al. 2007a,b); and the "fundamental metallicity relation" (e.g., Mannucci et al. 2010; Yates et al. 2012), were discovered in recent years. So far, many phenomenological models and numerical simulations can already reproduce some of these relations qualitatively, and in a few cases, quantitatively as well. A remarkable aspect of these relations is their small intrinsic scatter ($\leqslant 0.3$ dex) about the the mean trends.

The information contained in the scatter of these relations is not fully understood, but should provide additional insight into the galaxy formation processes (Salmi et al. 2012; Whitaker et al. 2012; Whitaker et al. 2015). For instance, the tight relation between M_* and star formation rate (SFR) observed across a wide range of redshifts suggests that the star-formation within galaxies is a highly regulated process (but see Kelson 2014 for an alternative point of view), and enhanced SFR during mergers has a small effect on the total mass-buildup of the galaxies (Noeske et al. 2007b). The small intrinsic scatter of the fundamental plane of early-type galaxies sheds light on the variety of stellar populations of these galaxies (Prugniel & Simien 1996; Forbes et al. 1998; Gargiulo et al. 2009; Graves et al. 2010; Taranu et al. 2015). Likewise, scatter in the M_*–size relation appears to be small and constant since $z \sim 2$ (van der Wel et al. 2014), which provides constraints on simple dry merger models (Nipoti et al. 2012). It is not known to what extent the scatter in these relations is due to different evolutionary pathways or to intrinsically stochastic processes (Kelson 2014).

By connecting dark matter halos with the properties of galaxies we can understand how the hierarchical growth of structure regulates the properties of galaxies. One powerful tool to link galaxy properties to the underlying dark matter halos is the stellar mass-halo mass (SMHM) relation. The mass ratio between the stellar content in the galaxy and its dark matter halo tells us how efficient the baryonic component has been converted into stars. To fully understand the origin of this relation and its intrinsic scatter, one needs to understand both the hierarchical growth of structures and the baryonic processes involved.

An accurate estimation of both the stellar mass and halo mass is a difficult task. Empirical estimates of the SMHM relation are conducted by both direct and indirect methods. Direct measurements include X-ray observations, Sunyaev-Zel'dovich effect, galaxy-galaxy lensing and satellite kinematics within galaxy clusters (e.g., Lin & Mohr 2004; Yang et al. 2007; Hansen et al. 2009; Kravtsov et al. 2014). Indirect methods include halo occupation distribution (HOD) modeling (Leauthaud et al. 2011, 2012; Zehavi et al. 2011; Parejko et al. 2013; Guo & White 2014; Yang et al. 2003), the conditional luminosity function modeling (Yang et al. 2009) and the abundance match-

[1] Department of Astronomy, Harvard University, Cambridge, MA 02138
[2] Space Telescope Science Institute, Baltimore, MD 21218, USA
[3] Department of Astronomy, University of California at Berkeley, Berkeley, CA 94720
[4] Hubble Fellow

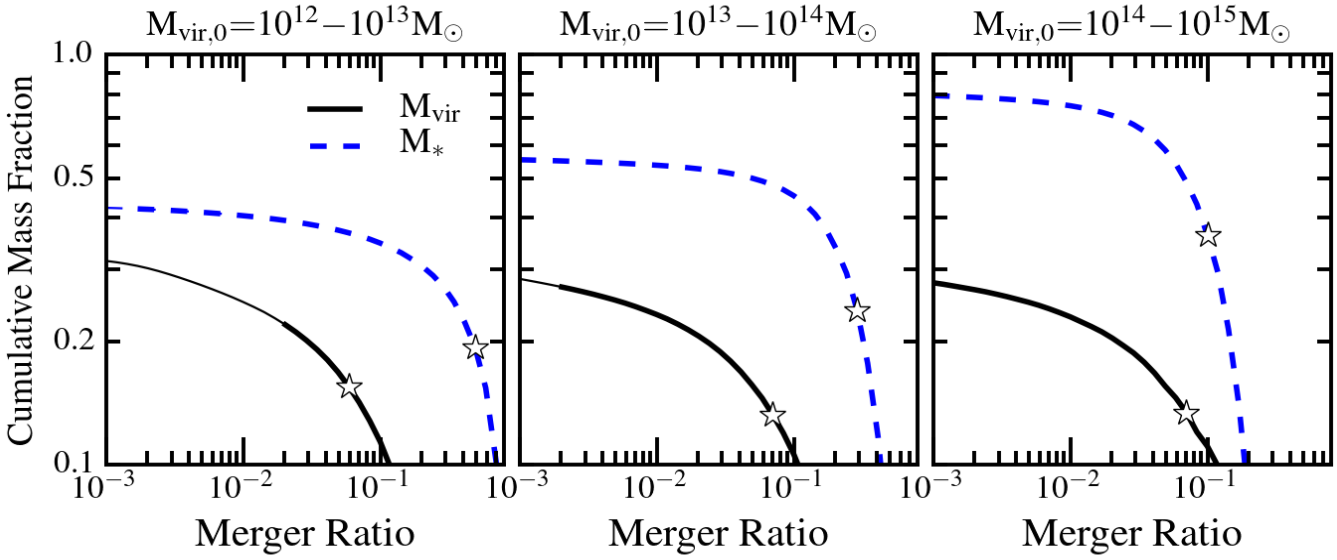

Figure 1. Cumulative stellar and halo mass fraction from accreted objects between $z = 2$ and 0 with merger ratio $> m/M_0$ where M_0 is the final mass at $z = 0$. The three panels show the cumulative mass contribution from mergers for the local host halos at different scales. Blue dashed lines and black solid lines show the stellar mass and halo mass fraction, respectively. Note the black lines do not include satellite halos that still retain their identity at $z = 0$. Thinner lines mark regions below the resolution limit of $2 \times 10^{10} M_\odot$ and the corresponding stellar mass resolution limit estimated using the SMHM relation from Behroozi et al. (2013c). The dark matter halo merger fractions are expected to be nearly self-similar. The cumulative mass fractions do not converge to one at small mass ratios because of the exclusion of satellite halos and smooth accretion (for halo mass), and in-situ star formation (for stellar mass). Stars mark the merger ratios above which half of the accreted mass is contributed, indicating that most of the accreted objects are well resolved by the Bolshoi simulation. For example, the left panel shows that half of the accreted halo mass are through mergers with ratio above 0.06, and half of the stellar mass is accreted by mergers with ratio above 0.5.

ing technique (Colin et al. 1999; Kravtsov & Klypin 1999; Kravtsov et al. 2004; Tasitsiomi et al. 2004; Vale & Ostriker 2004; Shankar et al. 2006; Vale et al. 2006; Neyrinck et al. 2004; van den Bosch et al. 2005; Conroy et al. 2006; Conroy & Wechsler 2009; Behroozi et al. 2010; Guo et al. 2010; Moster et al. 2010; Hearin & Watson 2013; Reddick et al. 2013). The scatter in a SMHM relation can be directly estimated from samples that have direct dynamical halo mass estimates, or it can be constrained by galaxy clustering statistics, especially at the high mass end where the sensitivity of the observations to scatter is large (e.g., Zheng et al. 2005, 2007; Tinker 2007; Leauthaud et al. 2012; Reddick et al. 2013). All the observational constraints so far suggest that the SMHM relation has a remarkably small intrinsic scatter, that shows no evidence for variation with halo mass ($\lesssim 0.2$ dex scatter in stellar mass at fixed halo mass at $z = 0$), which is surprising given the complex merging history and the baryonic processes involved in galaxy formation. Simulations and semi-analytic models have recently begun to match observational constraints on the SMHM relation (e.g., Wang et al. 2006; Somerville et al. 2008; Guedes et al. 2011; Munshi et al. 2013). There has however been almost no work to date on understanding the constraining power contained in the observed *scatter* in the SMHM relation. This is the goal of the present work.

Here we model the evolution of the SMHM relation and its scatter induced by the hierarchical growth of dark matter halos from $z = 2$ to 0. We focus on distinct halos with $M_{\rm vir} > 10^{12} M_\odot$ at $z = 0$. During this complex mass assembly history, many processes (e.g., in-situ star formation, accretion of gas, stellar/AGN feedback) in addition to mergers affect the evolution of the SMHM relation. At the group and cluster scale ($M_{\rm vir} > 10^{14} M_\odot$), recent studies suggest that the bulk of their star formation activity has finished by $z \sim 2$, and their evolution after $z = 2$ is largely governed by dry mergers (e.g., van Dokkum & Franx 2001; Treu et al. 2005; Thomas et al. 2005; Choi et al. 2014; McDermid et al. 2015). For lower mass halos, in-situ star formation dominates the stellar mass growth. We therefore also explore the response of the scatter due to in situ mass growth. Our results indicate that the hierarchical growth of the dark matter structures induces a strongly mass-dependent scatter in the SMHM relation, and the addition of in-situ growth with an intrinsic scatter of 0.2 dex produces a scatter in the SMHM relation consistent with observations.

We assume a flat ΛCDM cosmology with $h = 0.70$, $\Omega_m = 0.27$, $\Omega_\Lambda = 0.73$, $\Omega_b = 0.0469$, $n = 0.95$. The halo mass in this paper, denoted by $M_{\rm vir}$, is defined as the mass enclosed within a spherical overdensity calculated from Bryan & Norman (1998). At $z = 0$ the overdensity is 360 times the background density. The stellar mass is denoted by M_*.

2. METHODOLOGY

2.1. *Bolshoi Simulation*

We make use of the Bolshoi simulation (Klypin et al. 2011), which is a large, dissipationless simulation of the evolution of the universe, assuming a flat, ΛCDM cosmology. The simulation adopted the cosmological parameters ($h = 0.70, \Omega_m = 0.270, \Omega_\Lambda = 0.730, \Omega_b = 0.0469, n = 0.95, \sigma_8 = 0.82$), consistent with the results from *WMAP*5 (Hinshaw et al. 2009; Komatsu et al. 2009; Dunkley et al. 2009) and *WMAP*7 (Jarosik et al. 2011; Komatsu et al. 2011). It followed 2048^3 particles in a comoving volume of $(250 h^{-1})^3$ Mpc^3 from $z = 80$ to $z = 0$. The evolution of the dark matter halos are recorded at 180 snapshots. The simulation has a mass resolution of $1.9 \times 10^8 M_\odot$ and a force resolution of $1 h^{-1}$ kpc. Assuming a conservative resolution limit of 100 particles (Behroozi et al. 2013d), the halo mass resolution limit is therefore roughly $2 \times 10^{10} M_\odot$, allowing us to study the prop-

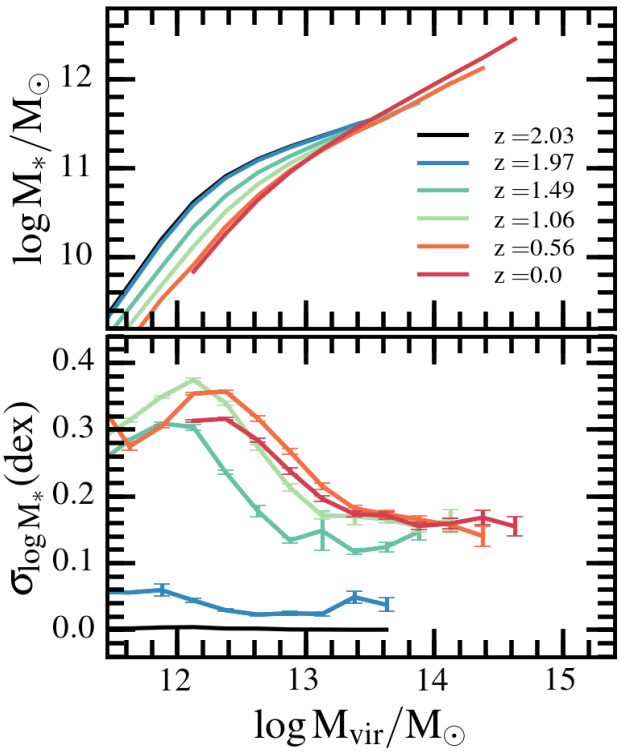

Figure 2. Evolution of the SMHM relation and scatter from $z = 2$ to $z = 0$ purely from hierarchical dark matter halo assembly (i.e., assuming that galaxies do not grow). The initial relation at $z = 2$ is adopted from Behroozi et al. (2013c). Error bars are determined by bootstrap resampling.

erties of dark matter halos with high accuracy.

In this work, we use the dark matter halos identified by the ROCKSTAR halo finder (Behroozi et al. 2013b). ROCKSTAR is based on adaptive hierarchical refinement of friends-of-friends groups, using not only the six phase-space dimensions but also the temporal dimension. Compared with other algorithms, it shows an advantage in probing substructure and maximizing the consistency of halo properties across time steps (Knebe et al. 2011). The halo catalogs and merger trees are generated by CONSISTENT TREES described in Behroozi et al. 2013e. This algorithm verifies the consistency of the halo finder and improves the completeness of the halo catalogs. It generates the dynamically consistent merger trees from the Bolshoi simulation with higher accuracy compared with particle based merger trees. We use the term subhalo as the halo identified in the virial radius of a larger halo. A halo is defined as a distinct halo if it's not within the virial radius of another halo.

2.2. *The Stellar Mass-Halo Mass Relation*

Associating galaxies with dark matter halos using the SMHM relation has been done by a variety of methods, including observations of individual objects, HOD modeling and abundance matching techniques. We use the SMHM relation provided by Behroozi et al. (2013c). The authors use a Markov Chain Monte Carlo method to model the SMHM from $z = 8$ to $z = 0$ with the aid of a variety of observational data, including the stellar mass functions, the distribution of specific star formation rates and the integrated cosmic star formation rates. The fitting function of the SMHM relations has 5 parameters, and can be described by a power law at the low mass end and a sub-power law at high mass. The specific form of the fitting function is

$$\log_{10}(M_*(M_{\rm vir})) = \log_{10}(\epsilon M_1) + f\left(\log_{10}\left(\frac{M_{\rm vir}}{M_1}\right)\right) - f(0)$$

$$f(x) = -\log_{10}(10^{\alpha x}+1) + \delta\frac{(\log_{10}(1+\exp(x)))^{\gamma}}{1+\exp(10^{-x})}$$

We adopt the best-fit parameters provided by Behroozi et al. (2013c). The resulting SMHM relation provides a good match to a wide array of observations from $z = 8$ to 0. In this work, we consider the satellite halos that may have a $M_{\rm vir}$ as low as a few times of the halo completeness limit, as well as the massive host halo more massive than $10^{14}M_\odot$. We therefore extrapolate the functional form of the SMHM beyond the observed mass range (Behroozi et al. 2013c). The extrapolation at the low-mass end does not show a noticeable impact on the mass growth, since there is only very little stellar mass content of the extrapolated galaxies.

Besides the stellar content in the galaxies, recent observations and simulations have demonstrated the important role of the intracluster light (ICL) component to the SMHM at the high-mass end (e.g., Lin & Mohr 2004; Gonzalez et al. 2007; Gonzalez et al. 2013; Zibetti et al. 2005). When a satellite galaxy disrupts, it is not clear what fraction of the stellar content will be deposited into the central galaxy versus the ICL. Meanwhile, it is also not clear whether the ICL can be seen as a separate component, and what is its best definition (kinematic or photometric). Recent observations suggest that the formation of the ICL strongly relates to past mergers (e.g., Gonzalez et al. 2013; DeMaio et al. 2015) so that part of the accreted stellar component between $z = 2$ to 0 must be in the ICL. In this work, we define the ICL as all the stellar components that are accreted onto the host halo but are not bound to the central galaxy. Behroozi et al. (2013c) provides two models of the SMHM relations across a wide range of redshifts. One model connects the host halos and the central galaxy, and the other uses a stellar component including both the central galaxy and the ICL. Throughout the paper, we adopt the SMHM relations including ICL as the fiducial model. We note that we have also explored a model using the SMHM without ICL and it does not alter our result of the scatter induced by hierarchical growth.

2.3. *Modeling Dissipationless Growth*

To isolate the scatter of stellar mass at fixed halo mass caused by galaxy mergers and mass accretion, we initially assume that the SMHM relation at $z = 2$ has no intrinsic scatter. (In Section 3.2, we consider a model in which the SMHM relation has a non-zero scatter.) We select a sample of distinct halos with $M_{\rm vir,z=0} > 10^{12}M_\odot$. For each distinct halo at $z = 0$, we trace back through its merger tree as a function of time up to $z = 2$ and find all of its progenitors at different epochs. The stellar masses of these distinct halos at $z = 2$ are calculated using its halo mass and the adopted zero-scatter SMHM relation at $z = 2$. For each progenitor that was accreted onto the host halo between $z = 2$ and $z = 0$, its stellar mass is estimated in a very similar way, using also a zero-scatter SMHM relation at the time of disruption, and the peak halo mass ($M_{\rm peak}$) of the progenitor. The peak halo mass is defined as the maximum halo mass in the progenitor's merger history. During the gradual disruption process of a progenitor, its dark matter content is stripped earlier than its baryonic component.

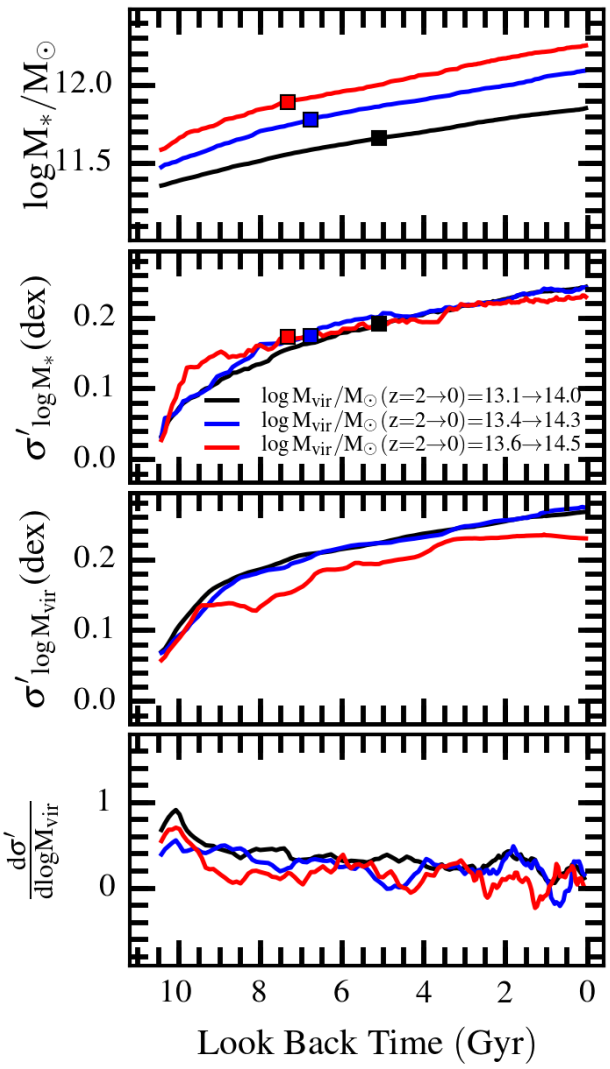

Figure 3. Evolution of the stellar mass and scatter in the three most massive bins from $z = 2$ to 0. From top to bottom, the stellar mass growth, the scatter in $\log M_*$, the scatter in $\log M_{\rm vir}$ and the change in scatter per unit $\log M_{\rm vir}$ are shown as a function of look back time. Squares indicate the time when the mean stellar mass is doubled. Note that the majority of the growth in the scatter occurs within the first mass doubling time.

Hence, the stellar mass of the progenitor should be unaffected in the early phase of the merger. The peak halo mass is therefore a better property to connect with the stellar component of the progenitor than the total halo mass right before disruption (e.g., Reddick et al. 2013).

Figure 1 shows the cumulative mass distribution of both the stellar component and the dark matter of the progenitors between $z = 2$ and $z = 0$ as a function of merger ratio. The halo mass in this figure refers to the mass just prior to the accretion. The stellar mass to halo mass ratio is not constant as a function of halo mass, therefore the stellar mass contribution from progenitors with different halo masses are not proportional. Thinner lines in Figure 1 show the regions below approximate halo mass resolution limit of 100 particles. For the two highest mass bins more than 90% of the mass is well resolved. Even for the lowest mass bin more than 50% of the accreted mass is resolved by the Bolshoi simulation.

2.4. *Modeling In-situ Growth*

Current models predict that the fraction of the total stellar mass contributed by accretion depends strongly on galaxy stellar mass. This fraction can be as large as above 80% for massive halos at group or cluster scale, but very small or even negligible for Milky Way-sized galaxies (e.g., Lee & Yi 2013; Rodriguez-Gomez et al. 2015; Purcell et al. 2007; Oser et al. 2010). As a result, hierarchical accretion should not be the dominant factor influencing the stellar mass scatter at the low mass end. For this reason, we include a model for the in-situ buildup of stellar mass. We assume that the final SMHM relation including both in-situ and ex-situ processes at $z = 0$ or $z = 1$ should be consistent with the result in Behroozi et al. (2013c). To estimate the in-situ stellar mass fraction, in each bin, we adopt a simplified assumption and take the average difference between the stellar mass from our hierarchical assembly model at $z = 0$ and the Behroozi et al. (2013c) model at $z = 0$ in this bin as the stellar mass growth due to in-situ star formation between $z = 2$ and $z = 0$. The in-situ stellar mass fraction includes both the initial stellar mass estimated using the SMHM relation at $z = 2$ and the subsequent in-situ growth estimated using the method described above. We estimate the in-situ stellar mass fraction at $z = 1$ in a similar way. The resulting $z = 0$ in-situ fraction is $\sim 19\%$ at $M_{\rm vir} = 10^{14} M_\odot$, reaches $\sim 52\%$ at $M_{\rm vir} = 10^{13} M_\odot$, and is $\sim 85\%$ at $M_{\rm vir} = 10^{12} M_\odot$.

We also consider a model in which the intrinsic scatter associated with the in-situ component has a value of $\sigma_i = 0.2$ dex. For the host halos, we assume that the initial stellar masses at $z = 2$ are formed in-situ and they follow a log-normal distribution with a scatter of 0.2 dex at fixed halo mass. The average in-situ growth after $z = 2$ is determined as the average difference between the stellar mass from our ex-situ model and the Behroozi et al. (2013c) model at $z = 0$. The average total stellar mass due to in-situ growth is the sum of the two. At $z = 0$, we assume that the total stellar mass due to in-situ growth of the host halo follow a log-normal distribution with a scatter of 0.2 dex at fixed halo mass. For the progenitors, we assume that the adopted initial SMHM relation is also a consequence of in-situ growth. The SMHM relations for progenitors between $z = 2$ and 0 hence also has a 0.2 dex scatter.

3. RESULTS

We now present our results. In Section 3.1, we show the SMHM relation and its scatter evolution driven by purely hierarchical assembly. We then discuss the possible factors that influence the growth of scatter in the case of purely dissipationless growth. In Section 3.2 we present results from the model including both ex-situ and in-situ processes. We compare our results with observational constraints in Section 3.3.

3.1. *Scatter due to Ex-situ Growth*

To isolate the influence due to mergers, we first construct a model with only hierarchical accretion. In this section, we present our fiducial ex-situ growth model, and then turn to an investigation into the variables affecting the scatter in the case of ex-situ growth. Several sources determine the final scatter in $\log M_*$. First, the shape of the SMHM relation determines the distribution of the stellar mass of satellite galaxies, which in turn influences the scatter in $\log M_*$. In Section 3.1.2, we study the relation between the slope of the SMHM relation at $z = 2$ and the scatter at $z = 0$. Second, the growth of dark matter halos due to smooth accretion plays an important role. We compare our results with and without smooth accretion in

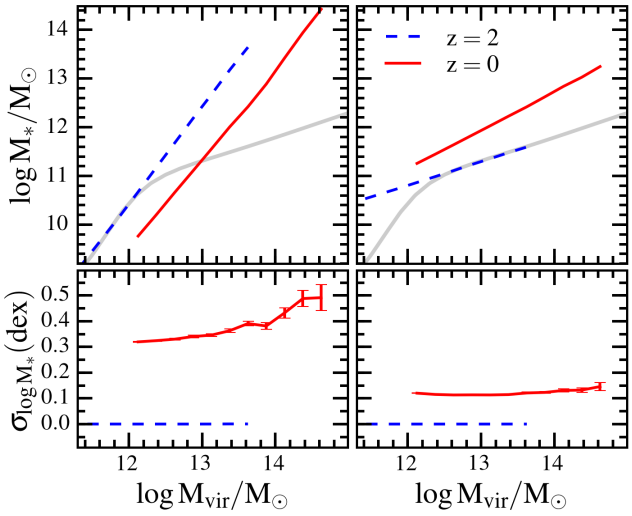

Figure 4. Comparison of the scatter in two hypothetical SMHM relations with single slopes. The slopes are identical to the low mass end and high mass end slopes in the SMHM relations from Behroozi et al. (2013c). Bottom panels show the evolved scatter (red) at $z = 0$. Note that they are sensitive to the slopes of the SMHM relations. A steeper slope at $z = 2$ results in a larger scatter of stellar mass at fixed halo mass at $z = 0$.

Section 3.1.3. Finally, massive halos on average experience more merger events than low mass halos. In Section 3.1.4, we show that the scatter of $\log M_*$ at fixed halo mass at $z = 0$ also depends on the number of merger events that a distinct halo has experienced.

3.1.1. *Fiducial Model*

Figure 2 shows the evolution with time of the SMHM relation and its scatter in our fiducial, ex-situ growth-only model. At $z = 2$, the SMHM relation has zero scatter at all halo mass. The stellar mass of the distinct halo gradually builds up through mergers since $z = 2$. When calculating the SMHM relations, we adopt a bin width of 0.25 dex in $\log M_{\rm vir}$. Only bins that contain more than 30 halos are included in our analysis. In order to compute the scatter, we linearly interpolate mean stellar mass between bin centers, then subtract off this mean relation before computing scatter. This avoids complications that would arise due to the shape of the SMHM relation and the width of the bins. The stellar mass and the scatter is the mean and standard deviation of $\log M_*$ of galaxies in each bin.

At $z = 1.97$, the first time step right after $z = 2$, a notable scatter of the SMHM relation is already apparent, especially at the low mass end. The scatter then builds up gradually and even shows a slight decrease later on at the high mass end. At $z = 0$, the scatter of the SMHM relation is strongly mass-dependent, reaching 0.32 dex at $M_{\rm vir} \sim 10^{12.5} M_\odot$, which is much larger than the 0.16 dex scatter at the high mass end.

To investigate the stellar mass growth in a small population of galaxies that share the same initial halo and hence stellar mass, we identify three groups of halos at $z = 2$ and follow their evolution to $z = 0$. The result is shown in Figure 3. We select the three most massive bins at $z = 2$ that contain more than 30 host halos. The bins are defined by $10^{13.0} M_\odot < M_{\rm vir} < 10^{13.25} M_\odot$, $10^{13.25} M_\odot < M_{\rm vir} < 10^{13.5} M_\odot$, $10^{13.5} M_\odot < M_{\rm vir} < 10^{13.75} M_\odot$ at $z = 2$, respectively. We trace each halo in each group from $z = 2$ to 0. Figure 3 shows the growth in $\sigma'_{\log M_*}$ and $\sigma'_{\log M_{\rm vir}}$ as a function of the look back time. It is worth mentioning that the $\sigma'_{\log M_*}$ here is different from the $\sigma_{\log M_*}$ in Figure 2. Here we trace the same host halos in each group from $z = 2$ to 0 and the mean $\log M_{\rm vir}$ changes with time, whereas in Figure 2 we study the host halos at fixed halo mass at each time step. The squares in Figure 3 show the time when the geometrically averaged stellar mass in each group is doubled with respect to $z = 2$. The group with a larger halo mass double their stellar mass earlier than the low mass groups. The scatter in all three groups increases quickly within the time the stellar masses are doubled, and then gradually slow down. The low mass group has a slightly larger final scatter than the high mass group.

3.1.2. *The Slope of the SMHM Relation*

In Figure 2, there is an obvious transition in the slope of the SMHM relation at around $M_{\rm vir} = 10^{12.5} M_\odot$. The scatter in $\log M_*$ shows a dramatic decrease at a similar halo mass, suggesting a connection between the slope of the SMHM relation and the scatter associated with ex-situ growth. To study the relation between the slope of the SMHM relations for both the distinct and satellite halos and the resulting scatter at $z = 0$, we construct two hypothetical SMHM relations that roughly describe the high mass end slope and the low mass end slope of our fiducial SMHM relation. They are shown in Figure 4.

The two hypothetical SMHM relations and their scatter at $z = 2$ are shown in blue. The fiducial SMHM relation is plotted as gray lines in the background a comparison. We assume that both the distinct halos at $z = 2$ and the progenitors between $z = 2$ to 0 follow the same SMHM relation. We note that these single power law relations are obviously in conflict with the data and are not used to reflect the actual evolution. We just use them as a toy model to show the effect of the slope on the scatter. We adopt the same approach described in Section 3.1.1 for computing the scatter. The SMHM relations and the scatter about the mean relation at $z = 0$ are shown in red. The slope of the SMHM relations for the initial host halos and the progenitors has a clear effect on the scatter at $z = 0$.

Overall a steeper SMHM relation for host and satellite halos produces a larger final scatter at $z = 0$. This is consistent with our fiducial model shown in Figure 2. As shown in Figure 1, while dark matter halos have a relatively self-similar distribution of progenitors, the accretion of the stellar component depends strongly on mass. This is due to the changing slope in the SMHM relation. For a fixed distribution of progenitor halos, a steeper slope implies a wide range of progenitor galaxies and hence a larger final scatter. A second reason is that the slope of the SMHM relation influences the relative importance of major vs. minor mergers. A steeper SMHM relation produces fewer major mergers given the same dark matter assembly history, and hence increases the Poisson scatter.

3.1.3. *Effect of Smooth Accretion*

Part of the halo mass growth is associated with a diffuse component, i.e. the growth of dark matter halos due to smooth accretion. This contributes about 40% to the total growth of the dark matter halo (e.g. Stewart et al. 2008; Genel et al. 2010). Here we show that the smooth accretion is another factor influencing the scatter at $z = 0$.

In Figure 5, we compare results with different initial SMHM relations at $z = 2$, including or not the growth of the dark matter halo due to smooth accretion. All of the work up to this point has included smooth accretion of dark matter as a component of the total growth. The smooth accretion is also the major reason that the black lines in Figure 1 do not

converge to one at small mass ratios. To estimate the scatter without the influence of smooth accretion, we assume that the final halo mass of the distinct halo at $z = 0$ is the total virial mass of the progenitors at the time just prior to the accretion. The stellar mass is calculated in the same way as described in Section 2.3, i.e., it's the total stellar mass of progenitors based on their peak halo mass, and the SMHM relations at the time of disruption. Therefore the halo mass growth of distinct halos is solely due to the halo mergers, and the stellar mass of the central galaxy at any time is just the total stellar mass in the progenitors disrupted before that time.

In the top two panels we assume a SMHM relation with a fixed ratio between halo mass and stellar mass at $z = 2$ for both distinct halos and subhalos. If there were no smooth accretion of dark matter, we would predict that the ratio between $M_{\rm vir}$ and M_* should remain almost constant after mergersâĂŤexcept for a tiny variation due to mass ejection during major mergers (Behroozi et al. 2013a, 2015). The scatter in the SMHM relation is then expected to be nearly 0. This scenario is shown in the top left panel. It results in an almost uniform and very small scatter in $\log M_*$ at fixed halo mass at $z = 0$. We assign the stellar mass based on peak halo mass. The very small scatter in the top left panel comes from the difference between the peak mass and virial mass of satellites. However, when the growth of dark matter halos due to smooth accretion is included, the scatter grows to about 0.2 dex from $z = 2$ to $z = 0$, as shown in the top right panel. Comparing the two top panels, we conclude that part of the final scatter in $\log M_*$ can be attributed to the variation in the final halo mass due to smooth accretion. In other words, even for a model in which the stellar mass did not grow but the halos grew via smooth accretion, one would expect the scatter in stellar mass *at fixed halo mass* to increase over time.

Smooth accretion also has an effect on the scatter for our fiducial SMHM relation. This is shown in the bottom two panels of Figure 5, where the smooth accretion induces an increase in scatter of about 0.1 dex in host halos with M_* between $10^{13}M_\odot$ and $10^{14}M_\odot$, and a much larger increase in scatter at low mass host halos.

3.1.4. *Number of Merger Events*

We next consider the effect of the number of mergers on the scatter in stellar mass. To do this we set up a simple Monte Carlo simulation for the growth of stellar mass and scatter as a function of the number of merger events. We compare the evolution of two groups of halos with different initial virial mass, $M_{\rm vir} = 10^{12.6}M_\odot$ and $M_{\rm vir} = 10^{13.6}M_\odot$. Each group contains 500 halos. We construct a sample of progenitors for each group using the ROCKSTAR halo catalog of the Bolshoi simulation. For example, the progenitor catalog of the $M_{\rm vir} = 10^{12.6}M_\odot$ group consists of all the progenitors between $z = 2$ to 0 of the host halos with $M_{\rm vir} = 10^{12.6}M_\odot$ at $z = 2$ in Bolshoi simulation. The top panel of Figure 6 shows the mass weighted distribution of the progenitors' stellar mass. In this figure, the peak stellar mass of the progenitors is slightly higher for the high mass group. We use the number distribution of the progenitors in each group as a probability distribution and allow one progenitor to merge with the host halo at each step. The distributions are quite similar because of the shallow slope of the SMHM relation above $M_{\rm vir} \approx 10^{12.5}M_\odot$. The bottom panel of Figure 6 shows the evolution of the geometrically averaged stellar mass in each group.

For both groups, the scatter of $\log M_*$ quickly builds up to

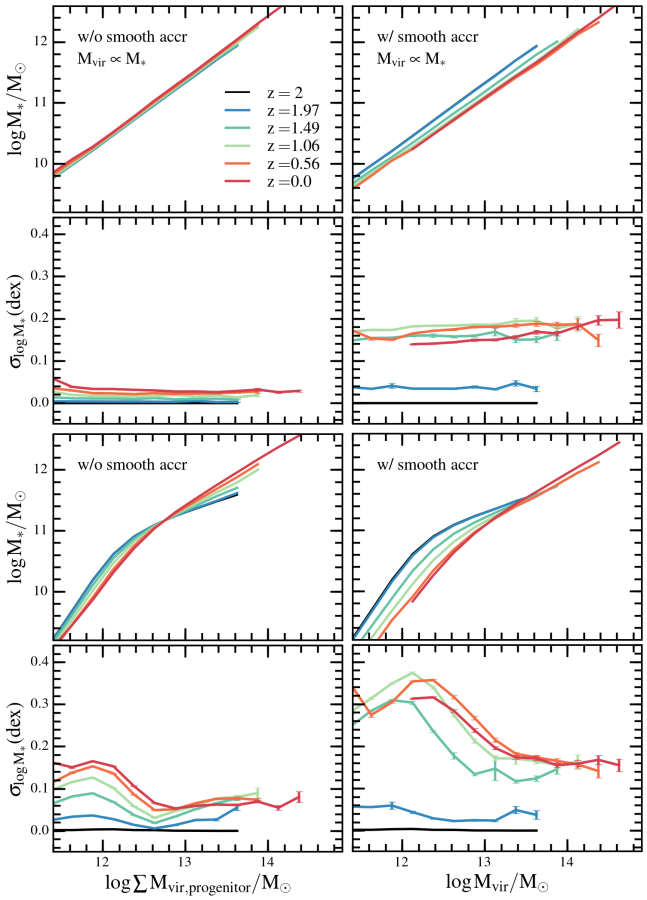

Figure 5. Impact of the shape of the SMHM relation and smooth accretion of dark matter on the scatter. Left panels and right panels show the result without and with smooth accretion. In the top panels we adopt a hypothetical SMHM relation in which the halo mass is proportional to the stellar mass. In the bottom panel we adopt the functional form of the SMHM relation from Behroozi et al. (2013c).

≈ 0.15 dex within the first 300 mergers, reaches a peak scatter near when the geometrically averaged stellar mass is doubled, and then slowly decreases. This behavior can be understood as follows. Initially the scatter is dominated by the in-situ mass, which by construction was initialized to be the same within each bin. Once the ex-situ mass becomes a major component but before there have been too many mergers, the scatter is large and influenced by the random draws from the progenitor distribution. Eventually, when the number of mergers is very large, each galaxy will have fully sampled the progenitor distribution and will therefore converge to the same mass in a central limit theorem-like process. The scatter produced from this simple model is similar with what is seen in our fiducial model (Section 3.1.1). This simple simulation reproduces the result that the scatter of $\log M_*$ is slightly smaller for the high mass group. This suggests that the scatter is sensitive to both the number of mergers and the mass function of the progenitors. Although not shown in Figure 6, the scatter will slowly decrease to zero eventually after $\sim 10^6$ mergers, when the stellar mass has increased by a factor of 10^3.

3.2. *In-situ Star Formation*

A generic expectation of modern galaxy formation models is that the mass buildup of galaxies is largely driven by in-

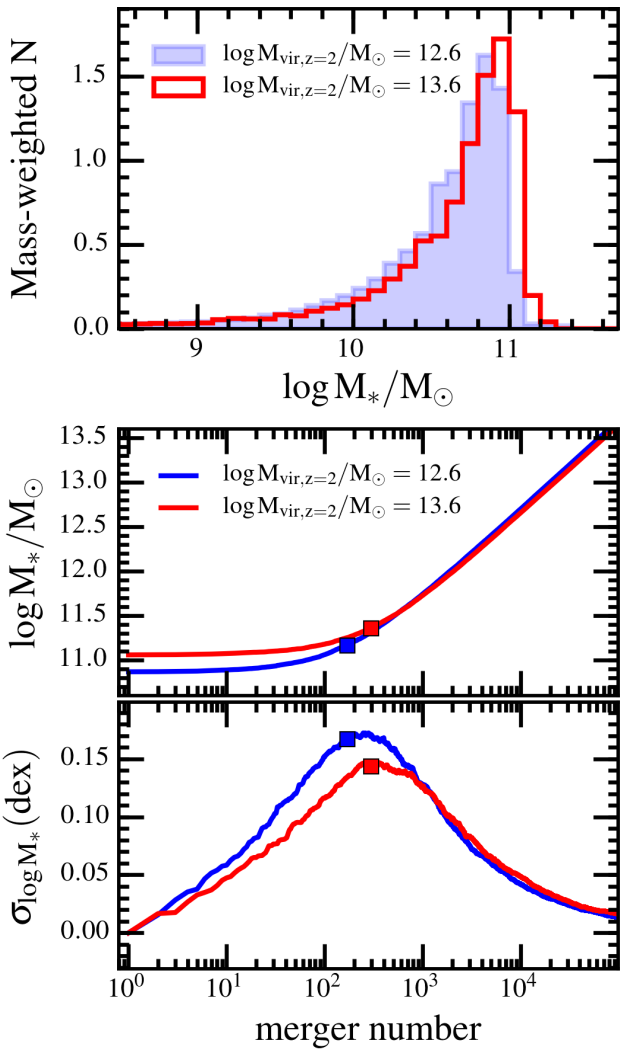

Figure 6. A simple Monte Carlo simulation for the stellar mass and scatter evolution due purely to hierarchical assembly in two halo mass bins. Each halo merges with a random progenitor at each step. Top panel shows the mass-weighted number distributions of progenitors of each halo mass bin. These distributions are the actual ones of progenitor masses for the halos in each mass bin in our fiducial model. Bottom panel shows the evolution of the average stellar mass and the scatter of 500 host halos as a function of the merger numbers. Squares indicate the point at which the mean stellar mass is doubled.

ternal (in-situ) processes at low masses and external (ex-situ) processes at high masses. In this section, we explore the response of the scatter in the SMHM relation to the combined effects of ex-situ and in-situ growth between $z = 2$ and 0. The in-situ model results in a final stellar mass that reproduces observational constraints (Behroozi et al. 2013b) by construction. We also include intrinsic scatter in the in-situ mode.

The effect of including in-situ growth is shown in Figure 7. Stellar mass growth due only to hierarchical assembly produces a final scatter of 0.16 dex at $M_{\rm vir} > 10^{14} M_\odot$ at $z = 0$, and even larger at lower masses (red line). We then include the stellar mass growth due to in-situ processes between $z = 2$ and 0 following the procedure described in Section 2.4, and assume that both the in-situ and ex-situ mass growth have no intrinsic scatter ($\sigma_i = 0$). The inferred total in-situ fraction is shown in the top panel of Figure 7. The final scatter of the SMHM relation is shown in blue. At the high mass end, it's very similar to our merger model, since the in-situ growth after $z = 2$ for cluster scaled halos is small. This indicates that the scatter in the SMHM relation at the group and cluster scale is mostly determined by ex-situ growth.

In addition to the diversity of merger histories, galaxies in dark matter halos of the same mass may experience different in-situ growth rates. One evidence of this is the well-defined relation between stellar mass and star formation rate, which has a scatter of ~ 0.3 dex. Therefore at fixed halo mass we might expect a dispersion of stellar mass due to in-situ processes. For this reason, we further consider a model in which the intrinsic scatter associated with the in-situ component has a value of $\sigma_i = 0.2$ dex. As described in Section 2.4, we assume that the total stellar masses due to in-situ growth at fixed halo mass at $z = 0$ have a scatter of $\sigma_i = 0.2$ dex for host halos. The stellar masses of progenitors between $z = 2$ and 0 at fixed halo mass also have a scatter of $\sigma_i = 0.2$ dex. In Figure 7, we plot the final scatter for host halos at $z = 0$ for the $\sigma_i = 0.2$ dex case in black. Since for low mass halos the mass buildup after $z = 2$ is driven largely by in-situ growth, the scatter at the low mass end is mainly determined by the in-situ scatter we assumed ($\sigma_i = 0.2$ dex). At the high mass end, the scatter is only slightly affected by the in-situ component. The overall scatter is almost flat as a function of halo mass. We show the result of the $\sigma_i = 0.3$ dex case in Figure 8.

3.3. *Comparison to Empirical Estimates of the Scatter*

We now turn to a comparison with observations. In Figure 8 we plot our model prediction for the scatter including the combined effect of in-situ and ex-situ stellar mass growth. We consider three values for the scatter due to in-situ processes: $\sigma_i = 0$, 0.2 dex and 0.3 dex. These three options are shown as dashed, solid and dotted lines.

First, we compare our result with direct observations. Kravtsov et al. (2014) presented measurements of the stellar mass and halo mass for 21 clusters using optical, infrared and X-ray data, and concluded that the relation between the stellar mass of the brightest cluster galaxies (BCGs) and M_{500} has a scatter of $\sigma_{\log M_{*,BCG}} = 0.17 \pm 0.03$. Patel et al. (2015) provided the SMHM relation measured for low mass groups between $0.5 \leq z \leq 1$. They found that the observed scatter of this relation is about $\sigma_{\log M_*} = 0.25$ dex. Note that their observed scatter included the uncertainty from the stellar mass measurement. The intrinsic scatter must be even smaller.

Some previous studies assumed that $\sigma_{\log M_*}$ is a constant for all halo mass. Leauthaud et al. (2012) studied the evolution of the SMHM relation from $z = 1$ to 0.2 by analyzing the galaxy-galaxy weak lensing, galaxy spatial clustering and galaxy number densities from the COSMOS survey. They had two models for the scatter. In the first model the $\sigma_{\log M_*}$ was assumed to be constant. In the second model, they assumed that the total scatter is the sum in quadrature of a constant intrinsic scatter and a mass-dependent scatter for the measurement error part. They fitted for the intrinsic scatter in the second model. They concluded that the two models produce very similar results. In Figure 8 we compare our result with the intrinsic scatter from their second model: $\sigma_{\log M_*} = 0.192 \pm 0.031$ dex at $0.22 \leq z \leq 0.48$ and $\sigma_{\log M_*} = 0.220 \pm 0.019$ dex at $0.74 \leq z \leq 1$. Yang et al. (2009) constrained the relation between halo mass and stellar mass of central galaxies using the observed stellar mass function provided by the galaxy group catalog from the SDSS DR4. They concluded the stellar mass distribution of galaxies at fixed halo mass can be described by a log-normal distribution

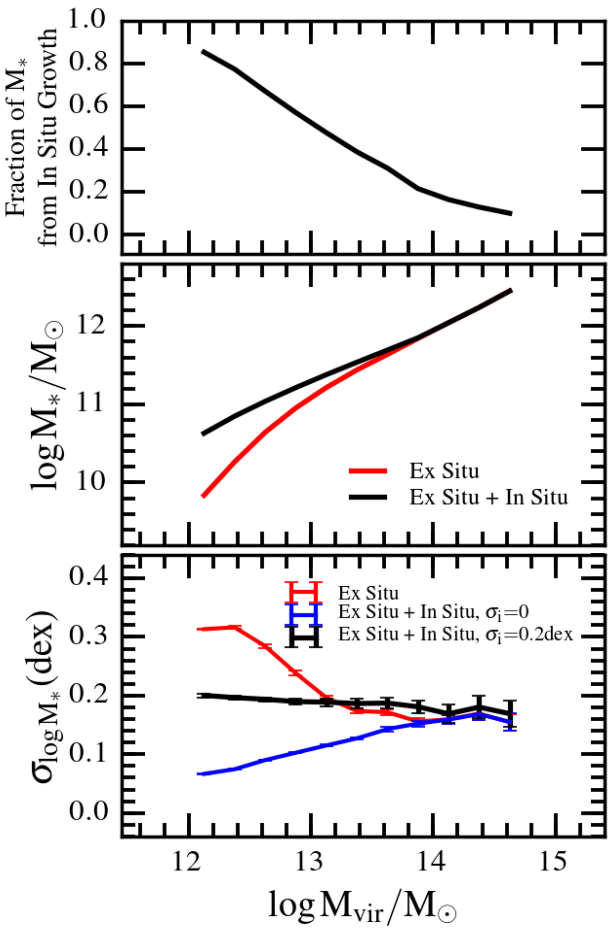

Figure 7. Behavior of models with and without in-situ mass growth. Top panel: The stellar mass fraction from in-situ growth as a function of halo mass at $z = 0$. Middle panel: The evolved SMHM relation at $z = 0$ solely driven by the hierarchical assembly of dark matter halos since $z = 2$(red), and by both ex-situ and in-situ processes (black). Bottom: The evolved scatter in $\log M_*$ at fixed halo mass at $z = 0$ solely driven by ex-situ processes (red), by both mergers and in-situ growth with zero intrinsic scatter (blue), and by both mergers and an in-situ growth with a 0.2 dex scatter (black).

and the scatter is roughly 0.17 dex. We compare our result with theirs from a combined sample of red and blue galaxies.

More et al. (2011) used the kinematics of satellite galaxies and the SDSS data to study the SMHM relation of central galaxies, and found the dependency of scatter on the color. They found that the scatter of halo mass at fixed stellar mass is constant for blue galaxies but increases as a function of stellar mass for red galaxies. Their results showed that $\sigma_{\log M_*} = 0.17^{+0.04}_{-0.03}$ dex for red central galaxies and $\sigma_{\log M_*} = 0.15^{+0.11}_{-0.08}$ dex for blue central galaxies. We only plot their result for red central galaxies in Figure 8 for simplicity. Tinker et al. (2013) also investigated the dependency on color at 3 redshift bins, $[0.22, 0.48], [0.48, 0.74], [0.74, 1]$. They constrained the SMHM relation for star-forming, and passive galaxies separately by combining constraints from the stellar mass function, the angular correlation function and galaxy-galaxy lensing from COSMOS data. In the low redshift bin, $\sigma_{\log M_*} = 0.21 \pm 0.06$ dex for star-forming galaxies and $\sigma_{\log M_*} = 0.28 \pm 0.03$ dex for passive galaxies. In the high redshift bin, $\sigma_{\log M_*} = 0.25 \pm 0.01$ dex for star-forming galaxies and $\sigma_{\log M_*} = 0.18 \pm 0.05$ dex for passive galaxies. In Figure 7 we compare our result with theirs for passive galaxies in their highest and lowest redshift bins.

Reddick et al. (2013) used subhalo abundance matching as well as constraints from the projected two-point galaxy clustering and the observed conditional stellar mass function to model the relation between the stellar mass and the peak circular velocity. They concluded that the peak circular velocity of the halos is the property that most closely connected to galaxy stellar mass, and the scatter in stellar mass at fixed peak velocity is $\sigma_{\log M_*} = 0.20 \pm 0.03$ dex. However, they also constrained the peak velocity-dependent scatter by only using the conditional stellar mass function for independent halo mass bins. They concluded that the scatter measured for the independent halo mass bins is consistent with their first model.

Lehmann et al. (2015) also conducted a subhalo abundance matching analysis by matching galaxy luminosity to halo properties. They included a new parameter, α, to control the dependence on concentration when halos are ranked by mass. They found a degeneracy between α and the log-normal scatter of galaxy luminosity. Moreover, their results show that the most important constraint of scatter is the clustering at high luminosity end, while clustering at lower luminosity ($\sim L_*$) mainly constrains α. They further assumed that both α and scatter are constant as a function of galaxy luminosity and found that best-fit value at $z = 0.05$ is $\sigma_{\log L} = 0.17^{+0.03}_{-0.05}$ dex.

Comparison between the data and our models suggests that the scatter associated with in-situ growth should be limited to ≈ 0.2 dex in order to reproduce a flat scatter in the SMHM relation from $10^{12} M_\odot < M_{\rm vir} < 10^{14.75} M_\odot$. At the group and cluster scale ($M_{\rm vir} > 10^{14} M_\odot$), the scatter in the SMHM relation is not sensitive to in-situ process and appears to be a generic outcome of hierarchical assembly of massive galaxies.

4. DISCUSSION

We have interpreted the scatter in the SMHM relation as a result of two distinct processes. At the high mass end the scatter is determined by hierarchical assembly, while at low masses the scatter is shaped by the intrinsic scatter associated with in-situ growth. Observations such as galaxy-galaxy lensing, satellite kinematics and galaxy clustering provide constraints on scatter for halos with $M_{\rm vir} > 10^{12} M_\odot$. They suggest that scatter associated with in-situ growth is limited to ≈ 0.2 dex. At high masses hierarchical growth also produces a scatter of ≈ 0.2 dex in stellar mass at fixed halo mass.

Our fiducial ex-situ growth model indicates that at $z = 0$, the scatter of the SMHM relation is strongly mass-dependent, reaching 0.32 dex at $M_{\rm vir} \approx 10^{12.5} M_\odot$ and 0.16 dex at $M_{\rm vir} \approx 10^{14.75} M_\odot$. This result alone has interesting implications. We should expect galaxies between 10^{10} to $10^{11} M_\odot$ to have larger scatter in their ex-situ stellar mass fraction. Assuming that most stars in the stellar halos come from ex-situ processes, our ex-situ only model provides a novel prediction for the scatter in the mass in the stellar halos. Upcoming surveys (e.g., van Dokkum et al. 2014) of stellar halo will help to constrain this picture.

The scatter of the SMHM relation contains valuable information on the galaxy formation process. It deserves careful consideration in both observations and simulations in the future. At the high mass end ($M_{\rm vir} > 10^{14} M_\odot$), the scatter is a generic consequence of the hierarchical assembly. Different simulations should be able to produce consistent scatter of the SMHM relation in this mass range. At lower halo mass

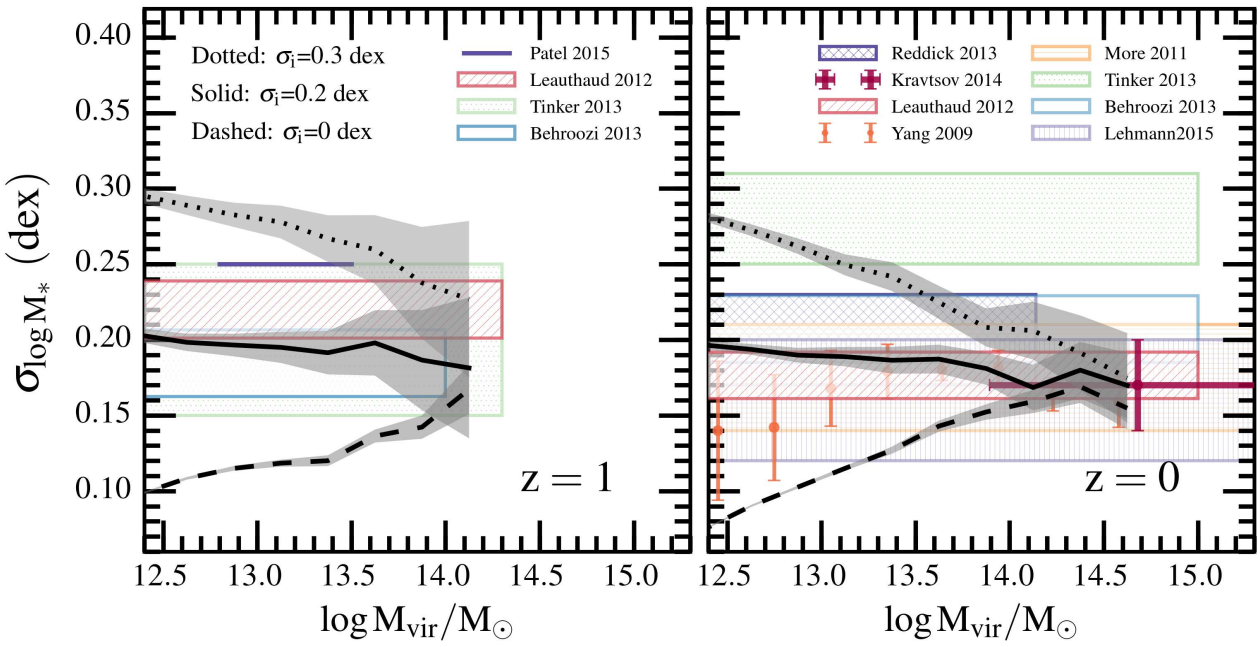

Figure 8. The scatter of stellar mass at fixed halo mass due to the combined effects from mergers and in-situ star formation. Left and Right panels show the predicted scatter from our models at $z = 1$ and $z = 0$ respectively, and are compared to observational estimates. Dotted, solid and dashed lines show the scatter assuming a 0.3 dex, 0.2 dex and zero dispersion in mergers and in-situ star formation, respectively. Shaded regions represent uncertainties of the scatter determined by bootstrapping.

($M_{\rm vir} < 10^{13} M_\odot$) the scatter gradually becomes dominated by baryonic processes involved in the in-situ build-up, and has potentially more constraining power on the underlying theory.

Two different processes, in-situ and ex-situ growth are needed to produce the apparent flat scatter in the SMHM relation. However the similar magnitude of the observed scatter at the low mass end and high mass end is likely a coincidence. Other works (e.g., Boylan-Kolchin et al. 2012; Garrison-Kimmel et al. 2014; Sawala et al. 2015; Dutton et al. 2015) have shown that at the regime of dwarf galaxies, the scatter of the SMHM relation may be much larger than in more massive systems. More stringent observational constraints on the mass dependence of the scatter would be valuable.

We end this section by highlighting several caveats and areas for future improvement. The Bolshoi simulation has a limited resolution (one particle mass = $1.9 \times 10^8 M_\odot$) and so halos with mass smaller than $2 \times 10^{10} M_\odot$ may not be properly described in the Bolshoi simulation. As shown in Figure 1, a fraction of satellite galaxies are possibly affected by this limited resolution. The result for host halo at the low mass end ($M_{\rm vir,z=0} < 10^{13} M_\odot$) should be treated with caution. However as discussed earlier, since the stellar component in such halos should be very small based on the SMHM relation, this should only have a small effect on our result. Moreover, we adopt a simple assumption that when a subhalo disrupts, all of its stellar content is accreted to the host halo, while in reality, the accretion of stellar mass could be delayed (Wetzel & White 2010). We also do not distinguish the stellar mass in the central galaxy and the ICL. Since most observations only include the stellar mass measurement of the central part of the host halo, a direct comparison with observations should also be treated with caution. The scatter in the SMHM relations observed should be roughly the quadratic sum of the intrinsic scatter discussed above and the measurement error. Behroozi et al. (2010) carefully studied different uncertainties in the SMHM relation. The authors included statistical uncertainties in the stellar mass function, cosmological parameters, and the uncertainty within the methodology to construct the SMHM relation, and revealed a ~ 0.07 dex (and ~ 0.12 dex) observational uncertainty at $z = 0$ (and $z = 1$). As shown in Figure 8, we compare with the observed scatter at $z = 0$ from Kravtsov et al. (2014). Even without the observational error, our fiducial model including a 0.2 dex scatter due to intrinsic process is already comparable with the observation at $z = 1$ and $z = 0$. If we consider the statistical errors provided by Behroozi et al. (2010), the intrinsic scatter could be even smaller.

5. CONCLUSIONS

We have used the Bolshoi simulation to study the origin of the scatter in the SMHM relation. We have included stellar mass growth both due to hierarchical assembly (ex-situ) and in-situ processes. Our main results are summarized as follows.

- The scatter due to hierarchical assembly is mass-dependent. At the group and cluster scale ($M_{\rm vir} > 10^{14} M_\odot$) the scatter due purely to mergers is $\approx$ 0.16 dex, which is very close to recent observational estimates. At lower halo masses ($M_{\rm vir} \sim 10^{12} M_\odot$) the scatter increases to 0.32 dex. Stellar halos, which are likely the result of this hierarchical assembly, may therefore show factors of ≈ 2 scatter from galaxy to galaxy at this mass range. (Section 3.1.1)

- Several factors influence scatter growth. The scatter is affected by the average number of mergers a population has experienced. The slope of the SMHM relation affects the scatter in a way that a steeper relations produces a larger scatter. The growth of dark matter halos

due to smooth accretion has a significant effect on the scatter growth. (Section 3.1.2-3.1.4)

- At lower masses, mass buildup since $z \approx 2$ is driven largely by in-situ growth. We include a model for the in-situ buildup of stellar mass. We find that an intrinsic scatter in this growth channel of 0.2 dex produces a relation between scatter and halo mass that is consistent with observations from $10^{12} M_\odot < M_{\rm vir} < 10^{14.75} M_\odot$. (Section 3.2-3.3)

The scatter in the SMHM relation is affected by two distinct processes: hierarchical assembly and in-situ growth. More precise observational estimates of the mass-dependent scatter should constrain both of these effects, and in particular should provide new insights into the regularity of the galaxy formation process.

We are grateful to Andrey Kravtsov and Risa Wechsler for helpful comments on an early draft. M.G. acknowledges support from the National Science Foundation Graduate Research Fellowship. C.C. acknowledges support from the Packard Foundation. P.B. was partially supported by a Giacconi Fellowship from the Space Telescope Science Institute. The remainder of support for P.B. through program number HST-HF2-51353.001-A was provided by NASA through a Hubble Fellowship grant from the Space Telescope Science Institute, which is operated by the Association of Universities for Research in Astronomy, Incorporated, under NASA contract NAS5-26555. The computations in this paper were run on the Odyssey cluster supported by the FAS Division of Science, Research Computing Group at Harvard University. This work made use of the Bolshoi simulation. The Bolshoi simulation has been performed within the Bolshoi project of the University of California High-Performance AstroComputing Center (UC-HiPACC) and were run at the NASA Ames Research Center.

REFERENCES

Behroozi, P., Knebe, A., Pearce, F. R., et al. 2015, MNRAS, 454, 3020
Behroozi, P. S., Conroy, C., & Wechsler, R. H. 2010, ApJ, 717, 379
Behroozi, P. S., Loeb, A., & Wechsler, R. H. 2013a, JCAP, 6, 019
Behroozi, P. S., Marchesini, D., Wechsler, R. H., et al. 2013b, ApJ, 777, L10
Behroozi, P. S., Wechsler, R. H., & Conroy, C. 2013c, ApJ, 770, 57
Behroozi, P. S., Wechsler, R. H., & Wu, H.-Y. 2013d, ApJ, 762, 109
Behroozi, P. S., Wechsler, R. H., Wu, H.-Y., et al. 2013e, ApJ, 763, 18
Blumenthal, G. R., Faber, S. M., Primack, J. R., & Rees, M. J. 1984, Nature (ISSN 0028-0836), 311, 517
Boylan-Kolchin, M., Bullock, J. S., & Kaplinghat, M. 2012, MNRAS, 422, 1203
Bryan, G. L., & Norman, M. L. 1998, ApJ, 495, 80
Choi, J., Conroy, C., Moustakas, J., et al. 2014, ApJ, 792, 95
Colin, P., Klypin, A. A., Kravtsov, A. V., & Khokhlov, A. M. 1999, ApJ, 523, 32
Conroy, C., & Wechsler, R. H. 2009, ApJ, 696, 620
Conroy, C., Wechsler, R. H., & Kravtsov, A. V. 2006, ApJ, 647, 201
DeMaio, T., Gonzalez, A. H., Zabludoff, A., Zaritsky, D., & Bradac, M. 2015, MNRAS, 448, 1162
Dunkley, J., Komatsu, E., Nolta, M. R., et al. 2009, ApJS, 180, 306
Dutton, A. A., Macciò, A. V., Frings, J., et al. 2015, ArXiv e-prints, arXiv:1512.00453
Forbes, D. A., Ponman, T. J., & Brown, R. J. N. 1998, ApJ, 508, L43
Gargiulo, A., Haines, C. P., Merluzzi, P., et al. 2009, MNRAS, 397, 75
Garrison-Kimmel, S., Boylan-Kolchin, M., Bullock, J. S., & Kirby, E. N. 2014, MNRAS, 444, 222
Genel, S., Bouché, N., Naab, T., et al. 2010, ApJ, 719, 229
Gonzalez, A. H., Sivanandam, S., Zabludoff, A. I., & Zaritsky, D. 2013, 778, 14
Gonzalez, A. H., Zaritsky, D., & Zabludoff, A. I. 2007, ApJ, 666, 147
González, V., Labbé, I., Bouwens, R. J., et al. 2010, ApJ, 713, 115
Graves, G. J., Faber, S. M., & Schiavon, R. P. 2010, ApJ, 721, 278
Guedes, J., Callegari, S., Madau, P., & Mayer, L. 2011, ApJ, 742, 76
Guo, Q., & White, S. 2014, MNRAS, 437, 3228
Guo, Q., White, S., Li, C., & Boylan-Kolchin, M. 2010, MNRAS, 404, 1111
Hansen, S. M., Sheldon, E. S., Wechsler, R. H., & Koester, B. P. 2009, ApJ, 699, 1333
Hearin, A. P., & Watson, D. F. 2013, MNRAS, 435, 1313
Hinshaw, G., Weiland, J. L., Hill, R. S., et al. 2009, ApJS, 180, 225
Jarosik, N., Bennett, C. L., Dunkley, J., et al. 2011, ApJS, 192, 14
Kelson, D. D. 2014, 1406.5191
Klypin, A. A., Trujillo-Gomez, S., & Primack, J. 2011, 740, 102
Knebe, A., Knollmann, S. R., Muldrew, S. I., et al. 2011, MNRAS, 415, 2293
Komatsu, E., Dunkley, J., Nolta, M. R., et al. 2009, ApJS, 180, 330
Komatsu, E., Smith, K. M., Dunkley, J., et al. 2011, ApJS, 192, 18
Kravtsov, A., Kravtsov, A. V., Vikhlinin, A., & Meshscheryakov, A. 2014, Stellar mass – halo mass relation and star formation efficiency in high-mass halos
Kravtsov, A. V., Berlind, A. A., Wechsler, R. H., et al. 2004, ApJ, 609, 35
Kravtsov, A. V., & Klypin, A. A. 1999, ApJ, 520, 437
Leauthaud, A., Tinker, J., Behroozi, P. S., Busha, M. T., & Wechsler, R. H. 2011, ApJ, 738, 45
Leauthaud, A., Leauthaud, A., Tinker, J., et al. 2012, ApJ, 744, 159
Lee, J., & Yi, S. K. 2013, ApJ, 766, 38
Lehmann, B. V., Mao, Y.-Y., Becker, M. R., Skillman, S. W., & Wechsler, R. H. 2015, ArXiv e-prints, arXiv:1510.05651
Lin, Y.-T., & Mohr, J. J. 2004, ApJ, 617, 879
Mannucci, F., Cresci, G., Maiolino, R., Marconi, A., & Gnerucci, A. 2010, MNRAS, 408, 2115
McDermid, R. M., Alatalo, K., Blitz, L., et al. 2015, MNRAS, 448, 3484
More, S., van den Bosch, F. C., Cacciato, M., et al. 2011, MNRAS, 410, 210
Moster, B. P., Somerville, R. S., Maulbetsch, C., et al. 2010, ApJ, 710, 903
Munshi, F., Governato, F., Brooks, A. M., et al. 2013, ApJ, 766, 56
Neyrinck, M. C., Hamilton, A. J., & Gnedin, N. Y. 2004, MNRAS, 348, 1
Nipoti, C., Treu, T., Leauthaud, A., et al. 2012, MNRAS, 422, 1714
Noeske, K. G., Faber, S. M., Weiner, B. J., et al. 2007a, ApJ, 660, L47
Noeske, K. G., Weiner, B. J., Faber, S. M., et al. 2007b, ApJ, 660, L43
Oser, L., Ostriker, J. P., Naab, T., Johansson, P. H., & Burkert, A. 2010, The Astrophysical Journal Letters, 725, 2312
Parejko, J. K., Sunayama, T., Padmanabhan, N., et al. 2013, MNRAS, 429, 98
Patel, S. G., Kelson, D. D., Williams, R. J., et al. 2015, ApJ, 799, L17
Peebles, P. J. E. 1982, ApJ, 263, L1
Prugniel, P., & Simien, F. 1996, Astronomy & Astrophysics, 309, 749
Purcell, C. W., Bullock, J. S., & Zentner, A. R. 2007, ApJ, 666, 20
Reddick, R. M., Wechsler, R. H., Tinker, J. L., & Behroozi, P. S. 2013, ApJ, 771, 30
Rodriguez-Gomez, V., Pillepich, A., Sales, L. V., et al. 2015, ArXiv e-prints, arXiv:1511.08804
Salmi, F., Daddi, E., Elbaz, D., et al. 2012, ApJ, 754, L14
Sawala, T., Frenk, C. S., Fattahi, A., et al. 2015, MNRAS, 448, 2941
Shankar, F., Lapi, A., Salucci, P., de Zotti, G., & Danese, L. 2006, ApJ, 643, 14
Somerville, R. S., Hopkins, P. F., Cox, T. J., Robertson, B. E., & Hernquist, L. 2008, MNRAS, 391, 481
Springel, V. 2005, MNRAS, 364, 1105
Stewart, K. R., Bullock, J. S., Wechsler, R. H., Maller, A. H., & Zentner, A. R. 2008, ApJ, 683, 597
Taranu, D., Dubinski, J., & Yee, H. K. C. 2015, ApJ, 803, 78
Tasitsiomi, A., Kravtsov, A. V., Wechsler, R. H., & Primack, J. R. 2004, ApJ, 614, 533
Thomas, D., Maraston, C., Bender, R., & Mendes de Oliveira, C. 2005, 621, 673
Tinker, J. L. 2007, MNRAS, 374, 477
Tinker, J. L., Leauthaud, A., Bundy, K., et al. 2013, ApJ, 778, 93
Treu, T., Ellis, R. S., Liao, T. X., et al. 2005, ApJ, 633, 174
Vale, A., & Ostriker, J. P. 2004, MNRAS, 353, 189
Vale, A., Vale, A., Ostriker, J. P., & Ostriker, J. P. 2006, MNRAS, 371, 1173
van den Bosch, F. C., Yang, X., Mo, H. J., & Norberg, P. 2005, MNRAS, 356, 1233
van der Wel, A., Franx, M., van Dokkum, P. G., et al. 2014, ApJ, 788, 28
van Dokkum, P. G., Abraham, R., & Merritt, A. 2014, ApJ, 782, L24
van Dokkum, P. G., & Franx, M. 2001, ApJ, 553, 90
Wang, L., Li, C., Kauffmann, G., & De Lucia, G. 2006, MNRAS, 371, 537
Wetzel, A. R., & White, M. 2010, MNRAS, 403, 1072

Whitaker, K. E., van Dokkum, P. G., Brammer, G., & Franx, M. 2012, ApJ, 754, L29
Whitaker, K. E., Franx, M., Bezanson, R., et al. 2015, ApJ, 811, L12
White, S. D. M., & Frenk, C. S. 1991, ApJ, 379, 52
White, S. D. M., & Rees, M. J. 1978, MNRAS, 183, 341
Yang, X., Mo, H. J., & van den Bosch, F. C. 2003, MNRAS, 339, 1057
Yang, X., Mo, H. J., & van den Bosch, F. C. 2009, ApJ, 695, 900
Yang, X., Mo, H. J., van den Bosch, F. C., et al. 2007, ApJ, 671, 153
Yates, R. M., Kauffmann, G., & Guo, Q. 2012, Monthly Notices of the Royal Astronomical Society, 422, 215
Zehavi, I., Zheng, Z., Weinberg, D. H., et al. 2011, ApJ, 736, 59
Zheng, Z., Coil, A. L., & Zehavi, I. 2007, ApJ, 667, 760
Zheng, Z., Berlind, A. A., Weinberg, D. H., et al. 2005, ApJ, 633, 791
Zibetti, S., White, S. D. M., Schneider, D. P., & Brinkmann, J. 2005, MNRAS, 358, 949